Physica E: Low-dimensional Systems and Nanostructures 101 (2018) 188–196

Contents lists available at ScienceDirect

Physica E: Low-dimensional Systems and Nanostructures

journal homepage: www.elsevier.com/locate/physe

Low-dimensional thermoelectricity in graphene: The case of gated graphene superlattices

S. Molina-Valdovinos *, J. Martínez-Rivera, N.E. Moreno-Cabrera, I. Rodríguez-Vargas

Universidad Autónoma de Zacatecas, Unidad Académica de Física, Calzada Solidaridad esq. Paseo, La Bufa s/n, CP 98060, Zacatecas, Zac, Mexico

ARTICLE INFO

Keywords:
Thermoelectricity
Graphene superlattices
Seebeck coefficient
Ballistic transport

ABSTRACT

Low-dimensional thermoelectricity is a key concept in modern thermoelectricity. This concept refers to the possibility to improve thermoelectric performance through redistribution of the density of states by reducing the dimensionality of thermoelectric devices. Among the most successful low-dimensional structures we can find superlattices of quantum wells, wires and dots. In this work, we show that this concept can be extended to cutting-edge materials like graphene. In specific, we carry out a systematic assessment of the thermoelectric properties of quantum well gated graphene superlattices. In particular, we find giant values for the Seebeck coefficient and the power factor by redistributing the density of states through the modulation of the fundamental parameters of the graphene superlattice. Even more important, these giant values can be further improved by choosing appropriately the angle of incidence of Dirac electrons, the number of superlattice periods, the width of the superlattice unit cell as well as the height of the barriers. We also find that the power factor presents a series of giant peaks, clustered in twin fashion, associated to the oscillating nature of the conductance. Finally, we consider that low-dimensional thermoelectricity in graphene and related 2D materials is promising and constitutes a possible route to push forward this exciting field.

1. Introduction

Thermoelectricity is a phenomenon that has captivated the minds of scientist for nearly 200 years. This fascination comes from the simplicity of the phenomenon, that is, by maintaining a temperature gradient it is possible to generate electricity. This exciting field formally started with the discovery of the Seebeck effect in 1821. Nowadays, there are a plethora of thermoelectric and thermomagnetic phenomena, for instance, the Peltier effect, Thomson effect, Nerst effect, Ettingshausen effect and Righi-Leduc effect [1]. Thermoelectricity remained without significant progress until the advent of semiconductors in the sixties of the last century. Semiconductors resulted ideal materials because they helped to increase the Figure of Merit, $ZT = S^2\sigma T/\kappa$, which is by far the most important quantity in thermoelectricity [2]. This quantity depends on the electric (σ) and thermal (κ) conductivities, the Seebeck coefficient (S) and the average temperature (T) between the hot and cold sides of a thermoelectric device. The relevance of this quantity comes from its direct relation with the efficiency of a thermoelectric device. In principle, there is no upper limit for ZT, and for large values of it, the thermoelectric efficiency will approach to the ideal Carnot efficiency. Then, the main issue for practical thermoelectric applications, that compete with traditionally power conversion technologies, is the rising of ZT. Until now there is no well defined theoretical limit for ZT, but in order to make thermoelectric devices competitive it is necessary that $ZT > 3$ [3]. However, for more than forty years the Figure of Merit of bulk semiconductors barely approached to 1 [4]. The most successful strategy was alloying [5]. With alloying a considerable reduction of the thermal conductivity was achieved, without detriment of the power factor ($S^2\sigma$). The interdependence of the Seebeck coefficient, electric and thermal conductivities is the main obstacle to reach and surpass the desirable value of 3 for ZT [6,7]. The best scenario for a thermoelectric material is that κ be reduced as much as possible and that the power factor be as large as possible, in other words, minimization and maximization, respectively.

In the dawn of 21st century a new concept burst the scene of thermoelectricity. This concept was based on low-dimensional structures such as quantum wells, wires and dots [8,9]. In fact, the name given to it was low-dimensional thermoelectricity [10–12]. It relies on the ability to redistribute the density of states (DOS) by changing the dimensionality of a semiconductor through size effects. Actually, DOS redistri-

* Corresponding author.
E-mail address: sergiom@fisica.uaz.edu.mx (S. Molina-Valdovinos).

https://doi.org/10.1016/j.physe.2018.03.005
Received 17 October 2017; Received in revised form 8 January 2018; Accepted 6 March 2018
Available online 17 March 2018
1386-9477/© 2018 Elsevier B.V. All rights reserved.

bution turns out in energy zones with accumulation of states. As the electric conductivity depends directly on DOS and as the Seebeck coefficient is a function of σ, the mentioned accumulation enhanced the power factor in unprecedented ways [13]. Furthermore, quantum wells, wires, and dots are typically arranged in a periodic fashion. This special arrangement also known as superlattices favours $S^2\sigma$ because represents an extra reduction of dimensionality [8,14]. Superlattices also reduce the thermal conductivity because the natural contrast between the building blocks of the superlattice structure serve as obstacle for thermal transport [15–17]. The net result of low-dimensional thermoelectricity is the improvement of the Figure of Merit to values close or even larger than the dreamed 3. For instance, quantum well superlattices of Bi_2Te_3/Sb_2Te_3, quantum wire superlattices of Si and quantum dot superlattices of PbSeTe give rise to Figures of Merit of 2.4, 1 and 1.6, respectively [15,18,19]. These outstanding improvements came to reinvigorate the field as well as allowing several thermoelectric applications.

On the other hand, the superb physical properties of cutting-edge materials like graphene are quite appealing for countless technological applications [20–22]. In specific, the excellent electric conductivity makes graphene a natural candidate for thermoelectricity. However, graphene, in reality, is a bad thermoelectric material due to its outstanding thermal conductivity [23]. For instance, suspended graphene [24] and graphene on hexagonal Boron Nitride [25] are among the materials with the highest mobilities, 200,000 $cm^2V^{-1}s^{-1}$ and $125,000\,cm^2V^{-1}s^{-1}$, respectively. The thermal conductivity is also high at room temperature, in the range of 2000–6000 $Wm^{-1}K^{-1}$, depending on the number of graphene layers [26,27]. These remarkable properties are closely related to the fundamental characteristics of graphene. This 2D material is a semi-metal with a gapless linear dispersion relation. The charge carriers behave as massless quantum relativistic particles known as Dirac electrons [20]. In the case of thermal transport, the most important contribution comes from the out-of-plane phonon modes. Under this context, how to do in order to transform graphene in a potential thermoelectric material. As in the case of semiconductors, the best strategy is to reduce dimensionality. One of the main proposals is based on the so-called graphene nanoribbons (GNRs). In these structures, the shape and edges dictate the fundamental properties [28–31]. So, by manipulating these structural characteristics it is possible to improve the Figure of Merit to values even superior to 3 [32,33]. Practically, all nanoribbons designs try to diminish the thermal transport without detriment to the power factor. Designs ranges from simple armchair GNRs [34,35], nanoribbons with mixed edges [36–38] to more elaborated chevron-type GNRs [32,39]. At this point, it is important to mention that despite the advance in the manipulation of the edges of GNRs [40,41], we consider that the sophistication of GNRs for thermoelectric applications would be problematic at experimental, and more importantly at mass production, levels. Another proposal that has been less explored and could have important possibilities is the one based on gating. Actually, by nanostructuring graphene with top gate electrodes in a periodic fashion, it is possible to obtain the so-called gated graphene superlattices (GGSLs) [42–45]. This nanostructuring, in principle, reduces dimensionality, redistributes the DOS and consequently can enhance the thermoelectric properties. In fact, giant values of the Seebeck coefficient, 30 mV/K and 260 mV/K, have been reported in GGSLs [46] and GGSLs with defects [47], respectively. Here, it is also important to remark that gated graphene structures are experimentally reliable at such degree that they have served as vehicles to test unprecedented phenomena like Klein tunneling [48,49]. For more details about the state of the art of thermoelectricity in graphene the reader is remitted to the excellent review of Dollfus et al. [50].

In the present work, we address the concept of low-dimensional thermoelectricity in graphene. In particular, we carry out a systematic assessment of the thermoelectric properties of quantum well GGSLs. We use the Dirac-like equation to describe the charge carriers and we implement the transfer matrix approach, Landauer-Büttiker formalism and Cutler-Mott formula to obtain the transmission, transport and thermoelectric properties, respectively. We find that the giant value of the Seebeck coefficient can be improved up to two orders of magnitude without the need of incorporate a defect barrier in GGSLs. This enhancement can be achieved by appropriately choosing the angle of incidence of the impinging electrons. We also find that the giant values of the Seebeck coefficient are preserved even when we sum up on all transmission channels. Furthermore, we obtain that the oscillatory nature of the conductance give rise to twin giant peaks in the power factor. One of the peaks is related to the increasing (decreasing) behaviour of the conductance (Seebeck coefficient), while the other peak is associated to the decreasing (increasing) trend of the conductance (Seebeck coefficient). It is also important to mention that in a typical configuration of gated graphene structures the graphene sheet is place on a substrate like SiO_2. This aspect could be quite relevant because it is known that the thermal conductivity of graphene on this kind of substrates drops up to three orders of magnitude [23]. Then, in principle, this diminution of the thermal conductivity and the giant values of the power factor in quantum well GGSLs can confabulate to give rise to significant Figures of Merit.

2. Model for thermoelectric device based on graphene superlattice

A prototypical GGSL consist of: a graphene layer supported by non-breaking-symmetry SiO_2 substrate and an array of periodic metallic electrodes that are coupled to graphene through a dielectric SiO_2 [46,47]. Through the electrodes, an external electrostatic field can be applied [42]. The main effect of the electrostatic potential is a shifting of the Dirac cones proportional to the field strength V_0. This shifting generates a periodic pattern of regions with (barriers) and without (wells) potential, see Fig. 1. The latter region has a potential $V_0 = 0$, a thickness d_W and the transport is owing to electrons (calling to this region n-type graphene). The former region has a potential V_0, thickness d_B and the transport is owing to holes (calling to this region p-type graphene). To know the actual profile of the barriers it is necessary to solve the electrostatic problem that underlies between graphene and the top and back electrodes. However, if the electron wavelength is large compared to the length over which the potential rises the edges of the barriers can be considered as sharp [51]. In our case the edges are assumed as sharp, so the barriers can be considered as perfectly abrupt, in other words, stepwise potential barriers. If we applied an electric current I between the two graphene-metal junctions (contacts A and B), then the contact A is heated and the contact B is cooled. With the help of thermocouples, we can measure the difference of temperature between the contact A and B [52]. This configuration can be used for electrical cooling (Peltier Effect). The same device can be used for the generation of a voltage due to a temperature difference between the contacts A and B (Seebeck effect). This is possible if a controlled temperature gradient is applied to the sample by microfabricated heater while the resulting thermally induced voltage ΔV is measured by the voltage probes to acquire the Seebeck coefficient [53].

The transport of charge carriers through GSL is ballistic, highly anisotropic and in extreme cases results in group velocities that are reduced to zero in one direction but are unchanged in the other direction [43]. Depending on the transversal wave vector or the angle of the electrons that impinge on the superlattice structure the propagation properties can be tuned readily. The transmission of electrons through the periodic n-p superlattice may resemble optical refraction at the frontier of the interfaces. The quantum characteristic of electrons allows that their wave nature takes place. Then, an electron approaching the interface from the n-side is partly reflected and partly transmitted to the p-side. The Fermi momentum plays the same role as the refractive index in optics, with the sign determined by the charge carriers, positive for electrons and negative for holes [54].

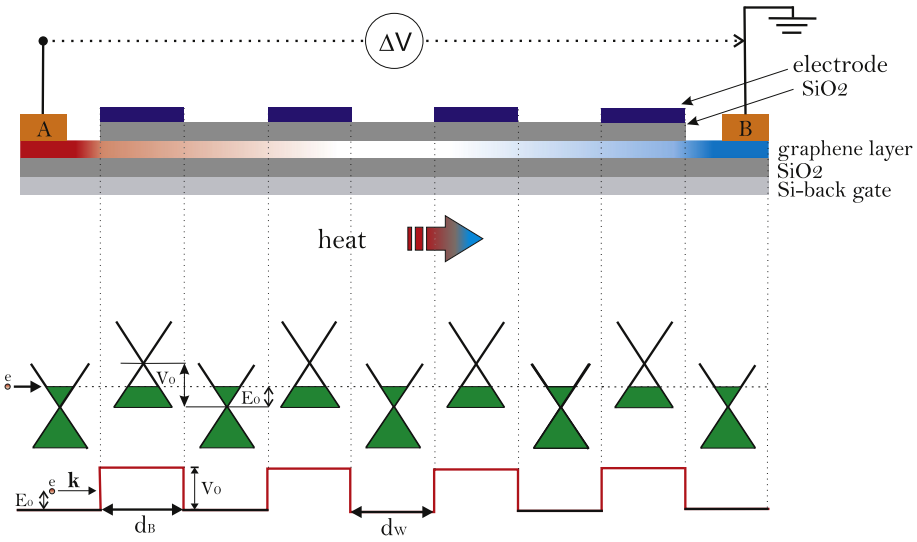

Fig. 1. (Top) Schematic representation for thermoelectric graphene devices based on p-n junction superlattices. The arrow indicates the direction of the heat flow, and ΔV denotes the voltage between electrodes. (Middle) Distribution of Dirac cones along the superlattice structure. (Bottom) Band-edge profile of the conduction band of GGSLs. V_0, d_B, d_W and E_0 represent the strength of the potential, the width of barriers and wells and the energy of an incident electron.

The massless Dirac-like equation describes this system and the shifting can be obtained through of:

$$[v_F(\vec{\sigma}\cdot\vec{p}) + V(x)]\psi(x,y) = E\psi(x,y), \tag{1}$$

where the components of pseudospin $\vec{\sigma} = (\sigma_x, \sigma_y)$ are Pauli matrices, $\vec{p} = (p_x, p_y)$ is the in-plane momentum operator, $V(x) = V_0$ is the one-dimensional potential along the x direction and $\psi(x,y)$ represents the wave function.

In the well and semi-infinite regions ($V(x) = 0$) the dispersion relation is given as $E = \pm\hbar v_F k$, while in the barrier regions an additional term appears due to the applied field, $E = V_0 \pm \hbar v_F q$. We denote the wave functions with $\psi^k_\pm(x,y)$ for the well and semi-infinite regions and $\psi^q_\pm(x,y)$ for the barrier regions:

$$\psi^k_\pm(x,y) = \frac{1}{\sqrt{2}}\begin{pmatrix}1\\ u_\pm\end{pmatrix} e^{\pm ik_x x + ik_y y}, \tag{2}$$

$$\psi^q_\pm(x,y) = \frac{1}{\sqrt{2}}\begin{pmatrix}1\\ v_\pm\end{pmatrix} e^{\pm iq_x x + iq_y y}, \tag{3}$$

where v_F is the Fermi velocity (for graphene $v_F = c/300$), k is the magnitude of the wave vector in the well and semi-infinite regions, k_x and k_y are the longitudinal and transversal components of k, $u_\pm = \pm s e^{\pm i\theta}$ the coefficients of the wave functions that depend on the angle of the impinging electrons, $\theta = \arctan(k_y/k_x)$ and $s = \text{sign}(E)$, $v_\pm = \frac{\hbar v_F(\pm q_x + iq_y)}{E - V_0}$, here V_0 is the strength of the electrostatic potential, q is the magnitude of the wave vector in the barrier regions, q_x and q_y are the components of q, and $v_\pm$ the coefficients of the wave functions.

We can apply the continuity conditions of the wave function along the superlattice axis as well as the conservation of the transversal momentum ($k_y = q_y$), and define the energy-dependent quantum transmission probability through the GGSL in terms of the so-called transfer matrix [55,56],

$$\mathbb{T}(E,\theta) = \frac{1}{|M_{11}|^2}, \tag{4}$$

which depends on the transfer matrices of barriers and wells, and the number of periods as well. The linear-regime conductance is obtained through the Landauer-Buttiker formula as [57]:

$$\mathbb{G}/G_0 = E_F^\star \int_{-\pi/2}^{\pi/2} \mathbb{T}(E_F,\theta)\cos(\theta)d\theta, \tag{5}$$

where $E_F^\star = E_F/E_0$ is the dimensionless Fermi energy with $E_0 = V_0$, $G_0 = 2e^2 L_y E_0/h^2 v_F$ is the fundamental conductance factor with L_y the width of the system in the transversal y-coordinate, and θ is the angle of the incident electrons with respect to the x-coordinate.

With the help of the conductance, we can compute the power or Seebeck coefficient in the low temperature limit and in absence of interactions [46,47]:

$$S(E,\theta) = -\frac{V}{\Delta T} = \frac{\pi^2 k_B^2 T}{3e}\frac{\partial \ln \mathbb{G}(E)}{\partial E}\bigg|_{E=E_F}, \tag{6}$$

where e is the electron charge, k_B is the Boltzmann constant, T is the average temperature between the hot and cold sides. In the case that, we have only a single conduction channel the Seebeck coefficient can be computed by changing $\mathbb{G}(E)$ for $\mathbb{T}(E,\theta)$ in equation (6). Note that for large values in ZT is necessary a large Seebeck coefficient, hence, the conductance or transmittance need a large variation at the Fermi energy.

3. Numerical results

Let us first calculate the transmission probability and the Seebeck coefficient of GGSLs as a function of the energy for different angles of incidence $\theta = 10°$, $30°$ and $60°$. The numerical results are presented in Fig. 2. The structural parameters considered for the superlattice were: an applied voltage $V_0 = 0.1$ eV, a maximum energy $E_{max} = 0.5$ eV, number of barriers $NB = 10$, barrier and well widths $d_B = 10$ nm and $d_W = 10$ nm, respectively.

As we can see for normal incidence $\theta = 0°$, the transmission probability is perfect ($\mathbb{T} = 1$, red line in Fig. 2a–c) and there is no formation of energy minibands and gaps (Klein tunneling). The Klein tunneling occurs when we have normal incidence, independent of the number of barriers, barriers width, or variation in applied voltage V_0 [45]. In this case, the Seebeck coefficient is zero, and consequently, the Figure of Merit is zero too. It means that charge carriers cross the superlattice from electrode A to electrode B, without a change in the transmission probability [58]. The superlattice structure does not contribute to improve the Seebeck coefficient.

In Fig. 2a–c, we can see that for small angles $\theta = 10^0$, we have pseudo minibands and gaps, since they are not well defined yet [58]. By increasing systematically the angle of incidence $\theta = 30°$, $60°$, we find that the mentioned pseudo minibands and gaps become well-defined ones. From Eq. (6) we can realize that in order to increase the Seebeck coefficient the term $(\partial \ln \mathbb{T}/\partial E)_{E=E_F}$ should be as large as possible. Thereby, in regions in which we have gaps, perfect transmission, maximums or minimums the Seebeck coefficient will be zero, see Fig. 2d–f. In the transition between minibands and gaps the Seebeck coefficient takes its maximum value, i.e., the change in $(\partial \text{In}\mathbb{T}/\partial E)|_{E=E_F}$ is large.

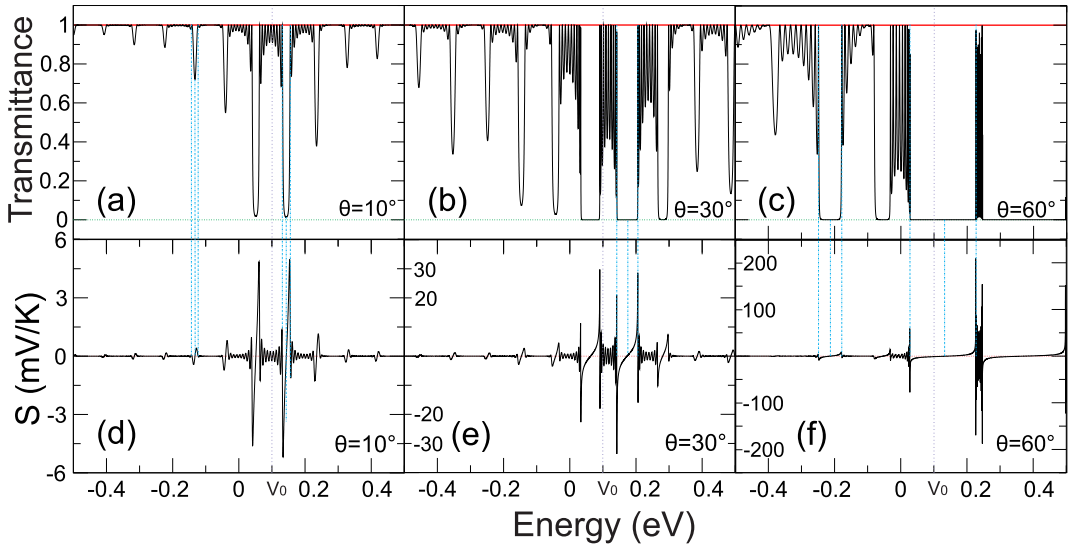

Fig. 2. Transmittance and Seebeck coefficient of GGSLs as a function of energy for different angles of incidence: (a) (d) $\theta = 10^{\circ}$, (b) (e) $\theta = 30^{\circ}$ and (c) (f) $\theta = 60^{\circ}$. The applied voltage, the number of barriers, the maximum energy and the widths of barriers and wells are $V_0 = 0.1$ eV, $NB = 10$, $E_{max} = 0.5$ eV and $d_B = d_W = 10$ nm, respectively.

Low values in S represent a small change in the transmission probability and high values in S are associated with large changes in the transmission probability. Under this context, the angle of incidence has a huge impact on the Seebeck coefficient because minibands and gaps are quite sensitive to this parameter, see Fig. 2a–c. In fact, minibands and gaps are not only well defined as the angle of incidence increases, they also become narrower and larger, respectively. These changes result in a systematic enhancement of the Seebeck coefficient. For instance, we obtain maximum values for the Seebeck coefficient of 5, 30 and 200 mV/K for angles of incidence of 10°, 30° and 60°, respectively. We can also notice the systematic change in sign of the Seebeck coefficient. This sign alternation is directly related to the reduce dimensionality of the system and not to the type of charge carrier as in bulk semiconductors. Such is the case that even when we have n-type, p-type or n-p type transport the sign alternation is preserved. In the present case of GGSLs the periodic modulation brought by itself specific characteristics on the transmission properties, minibands and gaps, that result in sign alternation.

GGSLs have different structural parameters that if appropriately chosen can help to improve the thermoelectric properties. Such is the case of the number of periods (barriers), the height of the barriers as well as the width of barriers and wells. The case of the number of barriers is quite useful because minibands and gaps can be better define by increasing the number of barriers even when the angle of incidence be small. In Fig. 3 we show the concrete results of the Seebeck coefficient for different number of barriers: (a) 3, (b) 6, (c) 10 and (d) 20. The angle of incidence considered is $\theta = 10^{\circ}$. The other structural parameters are the same as in Fig. 2. As we can notice for $NB = 3$ the Seebeck coefficient barely reaches a maximum value of 0.3 mV/K. We can also see a reduced number of peaks. The small values for the Seebeck coefficient are related to the lack of well define minibands and gaps, while the reduce number of peaks is associated to the reduce number of resonances within each miniband [56]. In fact, the number of resonances

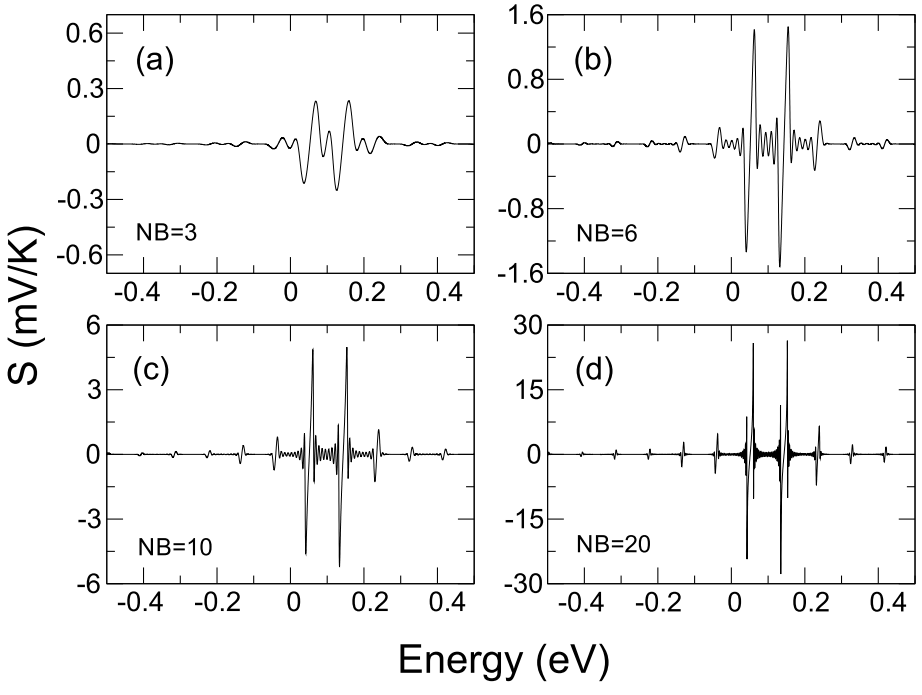

Fig. 3. Seebeck coefficient of GGSLs as a function of energy for different number of barriers: (a) $NB = 3$, (b) $NB = 6$, (c) $NB = 10$ and (d) $NB = 20$. The angle of incidence considered is $\theta = 10^{\circ}$. The other parameters are the same as in Fig. 2.

in each miniband is proportional to the number of wells in the superlattice. By increasing the number of barriers we can see an overall increase of the Seebeck coefficient and a multiplication of the number of peaks. In particular, we obtain maximum values for the Seebeck coefficient of 1.2, 4 and 26.38 mV/K, which correspond to number of barriers of 6, 10 and 20, respectively. Other interesting feature is that these maximum values are located at practically the same energy irrespective of the number of barriers. This can be understood by considering that an increase in the number of barriers does not entail a change in the width of minibands and gaps neither a shift of them, what really incorporates the number of barriers is a better definition of these superlattice characteristics specially at low energies.

Another parameter that can be used to tune the fundamental properties of GGSLs is the height of barriers. Contrary to what happen with the number of barriers the height of the potential allows us to increase the number of well defined minibands and gaps, to change the widths of minibands and gaps as well as to shift them. The specific results of the Seebeck coefficient for different barrier heights are shown in Fig. 4. In particular, we have considered heights of: (a) 0.1 eV, (b) 0.2 eV, (c) 0.4 eV and (d) 0.8 eV. Here, the number of barriers and the maximum energy considered are $NB = 10$ and $E_{\max} = 1.3$ eV. The angle of incidence and the width of barriers and wells are the same as in Fig. 3. From this figure, it is clear that the most important changes in the Seebeck coefficient are taking place at energies close to the height of the barriers. That's why we are seeing a shift to higher energies of the most important region in the Seebeck coefficient. By increasing the height of the barriers we are changing the degree of confinement in the structure and consequently changing practically all miniband structure characteristics. In the specific case of the maximum value of the Seebeck coefficient, we can see a systematic increase of this quantity as the barrier height grows. For instance, in the case of a single energy level, we get values of 5, 16, 35 and 41 mV/K for barrier heights of 0.1, 0.2, 0.4 and 0.8 eV, respectively.

At this point, it is important to remark that previous studies in GGSLs reported giant values for the Seebeck coefficient [46,47,59]. However, we are seeing here that a critical parameter to even improve the already giant values of the Seebeck coefficient in GGSLs is the angle of incidence. Even more important, if we combine appropriately the angle of incidence with the structural parameters of the superlattice we can obtain a further improvement of the Seebeck coefficient of two or even three orders of magnitude. As far as we know these values of tenths of V/K for the Seebeck coefficient are unprecedented for a solid-state structure. Despite of this, we consider that there are two important issues that we have to address in order to have a better understanding of the thermoelectric properties in GGSLs. The first one is related to the origin of the giant values of Seebeck coefficient as a function of the angle of incidence, and the second one to if the giant values are preserved when we sum up over all transmission channels, and more importantly if the power factor S^2G, which is the quantity that really matters for the figure of merit and consequently for the thermoelectric efficiency, also presents giant values.

To know the origin of the sensitivity of the Seebeck coefficient with the angle of incidence we will attend the fundamental aspect in low-dimensional thermoelectricity, that is, the redistribution of the density of states (*DOS*) with the reduction of dimensionality. And in the particular case of GGSLs also the variation of this quantity with the angle of incidence. We can obtain the $DOS(E,\theta)$ if we know the band structure of the superlattice, because there is a direct mathematical connection between these quantities [55], namely:

$$DOS^{*}(E,\theta) = \frac{DOS(E,\theta)}{L} = \frac{1}{2\pi}\left|\frac{\partial q_{SL}(E,\theta)}{\partial E}\right|, \tag{7}$$

where q_{SL} is the superlattice wave vector, $DOS^{*}(E,\theta)$ represent the number of states per unit length in a certain energy range and $DOS(E,\theta)$ represent the number of states in a certain energy range. The superlattice band structure can be computed by taking advantage of the direct relationship between the superlattice wave vector and the trace of the transfer matrix of the superlattice unit-cell [60],

$$2\cos(q_{SL}d_{SL}) = \mathrm{Tr}[M_{uc}], \tag{8}$$

here d_{SL} and M_{uc} represent the size and the transfer matrix of the unit cell, respectively. In our specific case the unit cell is compose of a barrier and a well, then, these quantities adopt the following values: $d_{SL} = d_B + d_W$ and $M_{uc} = M_B M_W$. Eq. (8) can be written explicitly as [60]:

$$\cos(q_{SL}d_{SL}) = \cos(q_x d_B)\cos(k_x d_W) + \frac{(\sin(\theta_B)\sin(\theta_W) - 1)}{\cos(\theta_B)\cos(\theta_W)}\sin(q_x d_B)\sin(k_x d_W),$$

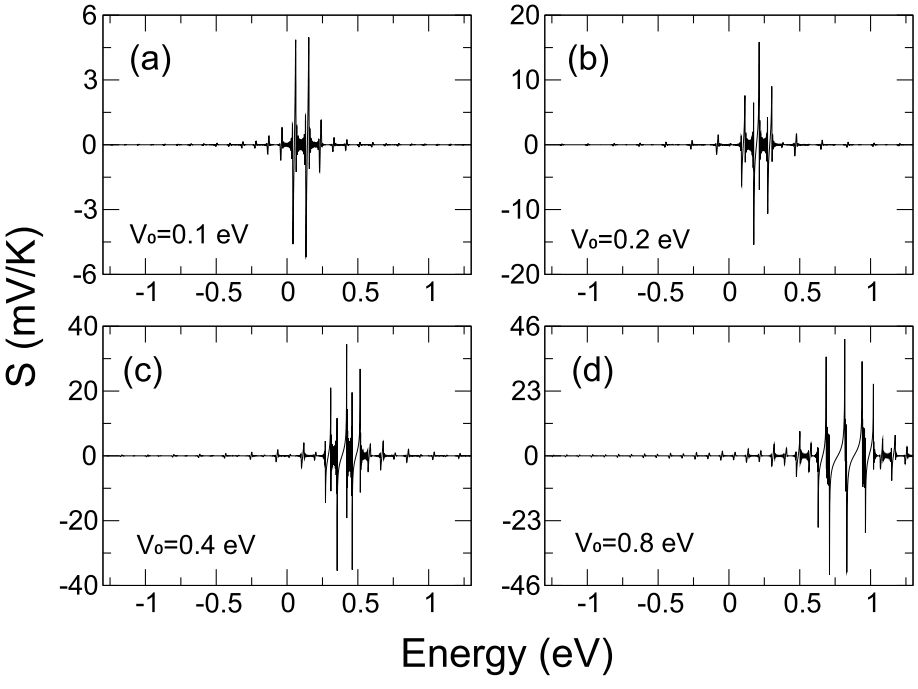

Fig. 4. Seebeck coefficient of GGSLs as a function of energy for different applied voltages: (a) $V_0 = 0.1$ eV, (b) $V_0 = 0.2$ eV, (c) $V_0 = 0.4$ eV and (d) $V_0 = 0.8$ eV. The maximum energy considered in this case is $E_{\max} = 1.3$ eV. The other parameters are the same as in Fig. 3.

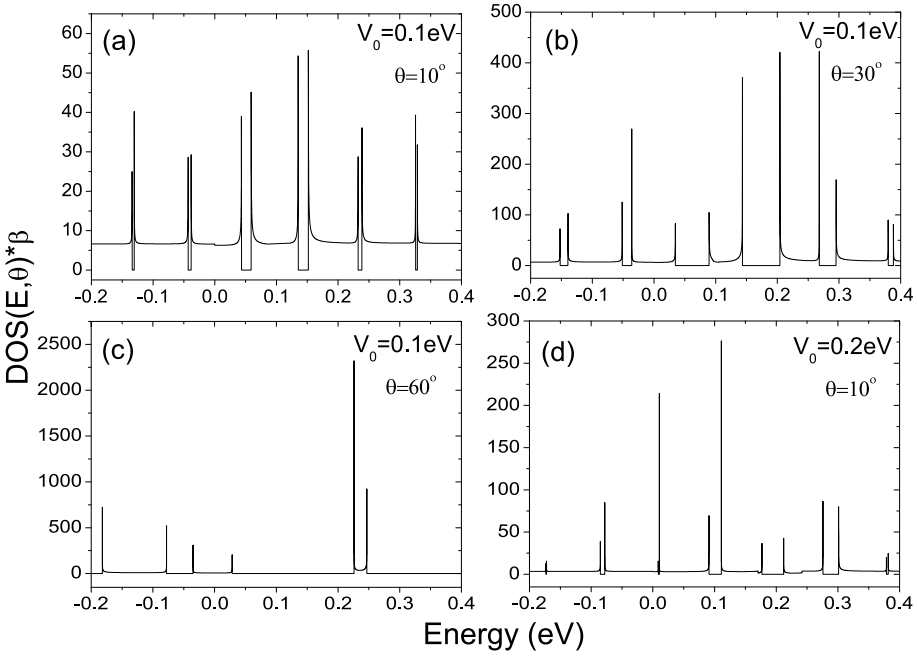

Fig. 5. Density of States $DOS(E,\theta)$ of GGSLs as a function of energy for different angles of incidence and different heights of the barriers: (a) $V_0 = 0.1$ eV, $\theta = 10°$, (b) $V_0 = 0.1$ eV, $\theta = 30°$, (c) $V_0 = 0.1$ eV, $\theta = 60°$, (d) $V_0 = 0.2$ eV, $\theta = 10°$. The size of the superlattice unit cell is $d_{SL} = 20$ nm, which corresponds to $d_B = d_W = 10$ nm. Here, β is equal to $\hbar v_F$. So, the vertical axis represents simply the number of states.

where θ_W and θ_B are the angles of the charge carriers in the well and barrier regions. For our system the angle in the well region coincides with the angle of incidence, $\theta_W = \theta$. The angle in the barrier comes in terms of the corresponding wave vectors $\theta_B = \arctan(q_y/q_x)$. Here, it is important to remark that the wave vectors of barrier and well regions depend on the energy and angle of incidence. Furthermore, the energies and superlattice wave vectors that represent the superlattice band structure are those that fulfill with the condition $|\mathrm{Tr}(M_{uc})| < 2$. Then, with the help of Eq. (9) it is possible to compute the density of states as a function of the energy.

In Fig. 5, we show our concrete results of the density of states for different angles of incidence and different heights of the barriers: (a) $V_0 = 0.1$ eV, $\theta = 10°$, (b) $V_0 = 0.1$ eV, $\theta = 30°$, (c) $V_0 = 0.1$ eV, $\theta = 60°$, (d) $V_0 = 0.2$ eV, $\theta = 10°$. In all these cases $d_B = d_W = 10$ nm. As it is expected in gap regions the density of states is zero. On the contrary, in miniband regions, the density of states is non zero and remains practically constant at the center of minibands. More importantly, we can notice accumulation of states at the edges of minibands. This accumulation is presented in practically all minibands, however, the accumulation is not the same in all them, and minibands with higher accumulation coincide with those at which the Seebeck coefficient gets its maximum values. We can also see that the density of states increases dramatically as the angle of incidence rises. For instance, when the angle changes from $\theta = 10°$ to $\theta = 30°$, the density of states increases around eight times, compare Fig. 5a and b. By increasing the angle of incidence to $\theta = 60°$ the density of states presents a further enhancement, about two orders of magnitude larger than the case of $\theta = 10°$, see Fig. 5c. By changing the applied voltage we can redistribute the

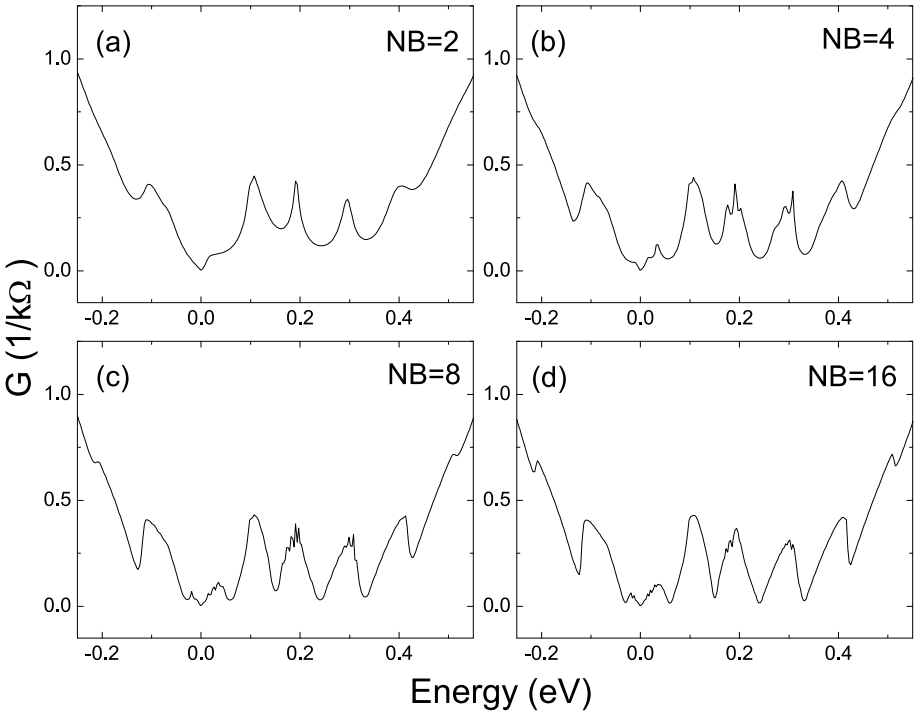

Fig. 6. Conductance of GGSLs as a function of the Fermi energy for different number of barriers: (a) $NB = 2$, (b) $NB = 4$, (c) $NB = 8$, (d) $NB = 16$. The other superlattice parameters adopt the following values: $d_B = d_W = 10$ nm, $E_0 = V_0 = 0.3$ eV and $E_{max} = 0.5$ eV. The lateral dimension of the structure is $L_y = 200$ nm.

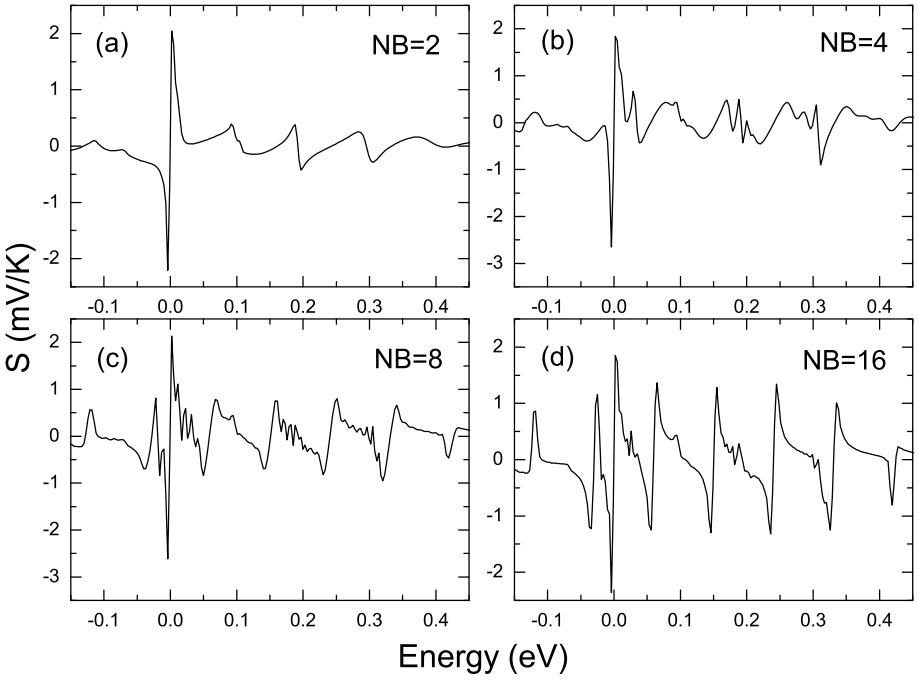

Fig. 7. Overall Seebeck coefficient as a function of the Fermi energy for different number of barriers: (a) $NB = 2$, (b) $NB = 4$, (c) $NB = 8$, (d) $NB = 16$. The other superlattice parameters are the same as in Fig. 6.

density of states such that the accumulation regions coincide with the maximums in the Seebeck coefficient, see Fig. 5d. Likewise, the rise of the barriers height enhances the density of states, see the vertical axis of Fig. 5d.

In order to unveil if after summing over all transmission channels the Seebeck coefficient as well as the power factor S^2G present giant values it is necessary to compute the linear-regime conductance. To this respect, in Fig. 6 we show the conductance of GGSLs for different number of barriers: (a) $NB = 2$, (b) $NB = 4$, (c) $NB = 8$ and (d) $NB = 16$. The other superlattice parameters remain fixed at: $d_B = d_W = 10$ nm, $E_0 = V_0 = 0.3$ eV and $E_{max} = 0.5$ eV. For the conductance it is necessary to specify the lateral dimension of the structure L_y, so we have chosen a typical value for gated graphene structures: $L_y = 200$ nm. As we can see the conductance oscillates as a function of the Fermi energy. Furthermore, the oscillations increase in number and become better define as the number of barriers grows. The main characteristic of the oscillations, maximums and minimums, can be ascribed to the opening and opening-closure of minibands as well as to the extra Dirac points in the electronic spectrum of GGSLs [44,61]. We can also see that the oscillations are not strictly speaking uniform, but they have some degree of periodicity that will be reflected in the Seebeck coefficient, see Fig. 7. This sort of periodicity is more evident as the number of barriers increases. In addition, the increasing and decreasing trend of the conductance will give rise to a Seebeck coefficient with decreasing and increasing regions and more importantly to possibly two closely spaced power factor peaks.

The concrete results of the Seebeck coefficient for all transmission channels are shown in Fig. 7. As we can notice the Seebeck coefficient remains giant after considering all channels, of the order of mV/K. It is clear that the values are not as giant as in the case of a single channel, but with respect to conventional materials, μV/K, we can still talk about giant values. When the number of barriers is small, for instance $NB = 2$, the dominant peaks in the Seebeck coefficient are associated to the graphene's Dirac point, $E = 0$. In fact, these peaks are four times greater than the peaks related to the periodic modulation, see the vertical scale in Fig. 7a. We can also see that the periodic pattern of the Seebeck coefficient is not well established when the number of barriers is small, see the cases of $NB = 2$ and $NB = 4$. As the number of barriers increases the peaks associated to the periodic modulation start to compete with the graphene's Dirac point peaks and the Seebeck's periodic pattern becomes better defined, see Fig. 7c and specially Fig. 7d. The Seebeck curves also present in general two preponderant regions: decreasing and increasing regions. The former span about 0.1 eV with a low decreasing rate, while the latter are steeper and with a high increasing rate. This is more evident in Fig. 7d. These characteristics, if appropriately combine with the conductance ones, can give rise to giant values of the power factor. In fact, in Fig. 8 we show the calculated power factor S^2G as a function of the Fermi energy for different number of barriers: (a) $NB = 2$, (b) $NB = 4$, (c) $NB = 8$ and (d) $NB = 16$. The other superlattice parameters are the same as in Fig. 7. At this point, it is important to remark that in bulk semiconductors it is well known that the increasing pace of the conductivity and the corresponding decreasing trend of the Seebeck coefficient give rise to a maximum in the power factor [7]. Here in GGSLs we have in addition to the mentioned peaks, extra ones related to the decreasing and increasing behaviour of the conductance and Seebeck coefficient, respectively. All these peaks are related to the oscillating character of the conductance, and at the end to the special characteristics of the electronic structure in GGSLs. As the increasing and decreasing conductance regions (oscillations) are close each other the corresponding peaks, in general, will arise in pairs. Indeed, a pair of peaks or twin peaks nicely arise in the case of $NB = 2$, see Fig. 8a. For GGSLs with larger number of barriers, the power factor curves at first instance are more irregular. However, if we inspect in more detail we can find multiple regions with pair of peaks. In some cases, the height of the peaks is almost the same, practically twin peaks, and in others the peaks are asymmetric with one being dominant. Other interesting and important feature is the systematic enhancement of the power factor as the number of barriers rises. The maximum value obtained for the power factor is around 200 pW/K^2, which represents a giant value if we consider the typical power factors reported in graphene nanoribbons 0.6 pW/K^2 [38].

4. Discussion

In the first place, we would like to discuss the experimental conditions for fabrication of the thermoelectric device proposed in the present work. The fabrication of electrode graphene superlattices, in principle, is possible due to the recent advances in nonscalable fabrication processes [62,63]. Actually, electrodes can be coupled to graphene trough dielectric SiO_2 layer with ultrashort top gate structures around

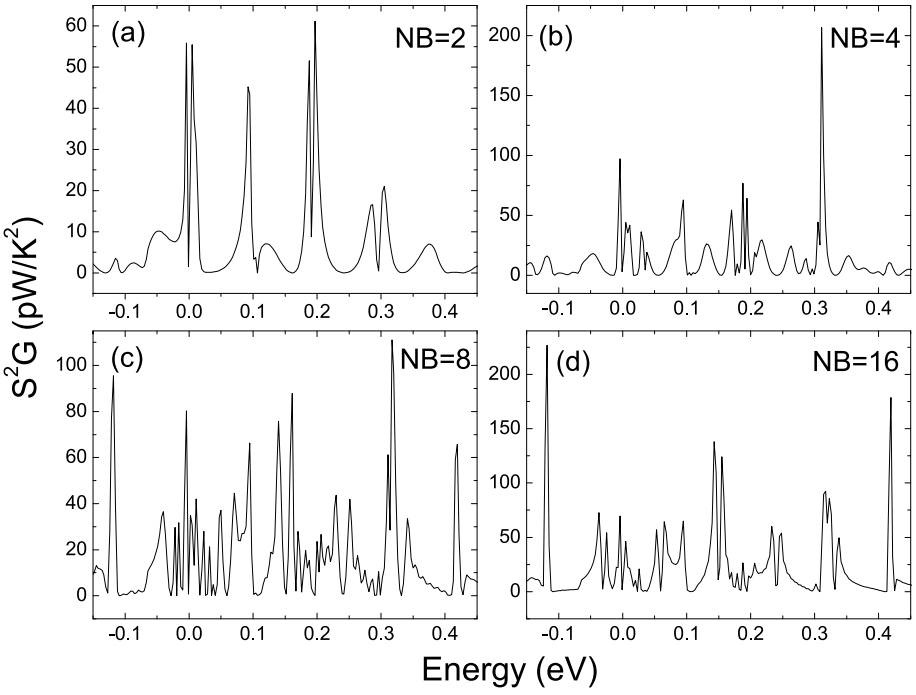

Fig. 8. Power factor S^2G as a function of the Fermi energy for different number of barriers: (a) $NB = 2$, (b) $NB = 4$, (c) $NB = 8$ and (d) $NB = 16$. The other superlattice parameters correspond to the ones of Figs. 6 and 7.

20 nm-100 nm, whose properties are sensitive to the top-gate oxide quality and thickness [63,64]. The metal contacts for source and drain consist of a metal stack of 20 nm Pd and 30 nm Au with the Pd layer in direct contact with graphene [62,64].

Second, we would like to talk about the thermal conductivity, given by $\kappa = \kappa_{el} + \kappa_{ph}$, where κ_{el} and κ_{ph} are the electron and phonon thermal conductivity. In metals, the high concentration of electrons, depending on the temperature range, can be the dominant contribution in thermal transport, $k_{el} \gg k_{ph}$. For instance, in copper $\kappa_{el} \sim 400$ WmK^{-1} at room temperature, while κ_{ph} is less than 1–2% of the total [6,65,66]. Nevertheless, in graphene, the principal contribution to the heat transport comes from phonons, $\kappa_{ph} \gg \kappa_{el}$. For suspended graphene, the in-plane thermal conductivity is around 2000–4000 $Wm^{-1}K^{-1}$ at room temperature [67]. Actually, this huge value of the thermal conductivity is one of the main hurdles to implement graphene as a thermoelectric material. If after placed the electrodes these values remain at the same order of magnitude the possible improvement of the power factor would be inconsequential to ZT, and consequently to the thermoelectric efficiency. Fortunately, there are multiple studies that report that the thermal conductivity can be diminished up to two orders of magnitude [23,68,69]. For instance, the thermal conductivity measured in graphene supported by SiO_2 was $\kappa_{ph} \sim 600$ $Wm^{-1}K^{-1}$ [23]. In addition, if graphene is encapsulated (SiO_2-encased graphene) an extra reduction, of a factor of 4, can be achieved $\kappa_{ph} \sim 160$ $Wm^{-1}K^{-1}$ [68]. In the case of supported GNRs the thermal conductivity barely reaches a value of ~ 80 $Wm^{-1}K^{-1}$ for 20-nm-wide samples [69]. Here, it is important to remark that all these reductions of the thermal conductivity are related in general to the coupling and scattering of graphene phonons with substrate vibrational modes [70]. Other aspect that could alter the phonon transport along the superlattice structure is the natural contrast between gated and non-gated regions. Regarding this point, it is well known that in superlattices of conventional materials such as GaAs/AlAs, Si/Ge, and Bi_2Te_3/Sb_2Te_3 the thermal conductivity is smaller than the corresponding one in its constituent single crystal materials [15,17,71,72]. In the case of graphene superlattices the large phonon mean free path can give rise to ballistic thermal transport, and as a consequence to the minimum thermal conductance phenomenon [73,74]. In particular, phonon confined modes and phonon wave interference in graphene-boron nitride superlattices can lead to minimum thermal conductance [75,76]. Regarding gated graphene superlattices, as far as we know, there is no report about thermal transport. However, minimum thermal conductance, as general phenomenon, it is also expected in this type of superlattices.

Finally, we would like to comment that the giant values of the thermoelectric properties in the single channel case are not in principle usable due to the difficulties that entail the incidence of electrons in a very specific angle. However, there are several groups trying to manipulate the propagation of Dirac electrons in graphene [77–79] as well as others trying to discriminate the angular contribution of the transmission properties across graphene p-n junctions [51,80–82]. So, it is possible that in the near future the propagation of Dirac electrons takes place, if not in a single channel (a specific angle of incidence), in a reduce number of them (reduce angular range). In any case, the giant values of the thermoelectric properties, for a single channel or for all channels, together with the small thermal conductivity in supported-encapsulated graphene constitute an interesting and attractive possibility for technological applications.

5. Conclusions

In summary, we have assessed the concept of low-dimensional thermoelectricity in graphene. In particular, we carried out a systematic study of the thermoelectric properties in quantum well gated graphene superlattices. The transfer matrix method, the Landauer-Büttiker formalism as well as Cutler-Mott formula have been used to obtain the transmission probability, linear-regime conductance and the Seebeck coefficient, respectively. We found that the Seebeck coefficient and the power factor reach giant values, three orders of magnitude, with respect to conventional quantum well superlattices. Even more important, these giant values can be further improved, up to two orders of magnitude, by appropriately choosing the fundamental parameters of the superlattice, specially the angle of incidence. As far as we have corroborated these outstanding results are intimately related to the central aspect in low-dimensional thermoelectricity, the redistribution of the density of states. We also found that the oscillating nature of the conductance gives rise to a series of giant twin peaks in the power factor. These giant values in conjunction with the drastic reduction of the thermal conductance of monolayer graphene when the graphene sheet is placed on a

substrate can confabulate to give rise to high values of the figure of merit and consequently high thermoelectric efficiencies. So, we firmly believe that low-dimensional thermoelectricity in graphene is a possibility that can reinvigorate this exciting field.

Acknowledgment

The Authors wish to thank CONACYT-México for partial financial support.

References

[1] D.M. Rowe, Thermoelectrics Handbook-macro to Nano, Taylor and Francis, Boca Raton, 2006.
[2] G.S. Nolas, J.W. Sharp, H. Goldsmid, Thermoelectrics: Basic Principles and New Matherials Developments, Springer, Berlin-Heidelberg, 2001.
[3] C.J. Vineis, A. Shakouri, A. Majumdar, M.G. Kanatzidis, Adv. Mater. 22 (2010) 3970–3980.
[4] A. Majumdar, Science 303 (2004) 777–778.
[5] H.J. Goldsmid, A.R. Sheard, D.A. Wright, Br. J. Appl. Phys. 9 (1958) 365–370.
[6] N. Stojanovic, D.H.S. Maithripala, J.M. Berg, M. Holtz, Phys. Rev. B 82 (2010) 075418.
[7] D. Rowe, CRC Handbook of Thermoelectrics, CRC-Press, 1995.
[8] L.D. Hicks, M.S. Dresselhaus, Phys. Rev. B 47 (1993) 12727–12731.
[9] D. Parker, X. Chen, D.J. Singh, Phys. Rev. Lett. 110 (2013) 146601.
[10] M.S. Dresselhaus, G. Dresselhaus, X. Sun, Z. Zhang, S.B. Cronin, T. Koga, Phys. Solid State 41 (1999) 679–682.
[11] M.S. Dresselhaus, G. Chen, M.Y. Tang, R. Yang, H. Lee, D.Z. Wang, Z. Ren, J. Fleurial, P. Gogna, Adv. Mater. 19 (2007) 1043–1053.
[12] J.P. Heremans, Acta Phys. Pol., A 108 (2006) 609.
[13] J.P. Heremans, B. Wiendlocha, A.M. Chamoire, Energy Environ. Sci. 5 (2012) 5510–5530.
[14] J.O. Sofo, G.D. Mahan, Appl. Phys. Lett. 65 (1994) 2690–2692.
[15] R. Venkatasubramanian, E. Siivola, T. Colpitts, B. O'Quinn, Nature 413 (2001) 597–602.
[16] D. Li, Y. Wu, R. Fan, P. Yang, A. Majumdar, Appl. Phys. Lett. 83 (2003) 3186–3188.
[17] S.M. Lee, D. Cahill, R. Venkatasubramanian, Appl. Phys. Lett. 70 (1997) 2957.
[18] A.I. Boukai, Y. Bunimovich, J. Tahir-Kheli, J.-K. Yu, W.A. Goddard III, J.R. Heath, Nature 451 (2008) 168–171.
[19] T.C. Harman, P.J. Taylor, M.P. Walsh, B.E. LaForge, Science 297 (2002) 2229–2232.
[20] A.H.C. Neto, F. Guinea, N.M.R. Peres, K.S. Novoselov, A. Geim, Rev. Mod. Phys. 81 (2009) 109–162.
[21] K.S. Novoselov, V.I. Fal'ko, L. Colombo, P.R. Gellert, M.G. Schwab, K. Kim, Nature 490 (2012) 192–200.
[22] A.C. F, et al., Nanoscale 7 (2015) 4598–4810.
[23] J.H. Seol, I. Jo, A.L. Moore, L. Lindsay, Z.H. Aitken, M.T. Pettes, X. Li, Z. Yao, R. Huang, D. Broido, N. Mingo, R.S. Rouff, L. Shi, Science 328 (2010) 213.
[24] K.I. Bolotin, K.J. Sikes, Z. Jiang, M. Klima, G. Fudenberg, J. Hone, P. Kim, H.L. Stormer, Solid State Commun. 146 (2008) 351–355.
[25] P.J. Zomer, S.P. Dash, N. Tombros, B.J.V. Wees, Appl. Phys. Lett. 99 (2011) 232104.
[26] A.A. Balandin, S. Ghosh, W. Bao, I. Calizo, D. Teweldebrhan, F. Miao, C.N. Lau, Nano Lett. 8 (2008) 902–907.
[27] S. Ghosh, W. Bao, D.L. Nika, S. Subrina, E.P. Pokatitov, C.N. Lau, A.A. Balandin, Nat. Mater. 9 (2010) 555–558.
[28] Y.-W. Son, M.L. Cohen, S.G. Louie, Phys. Rev. Lett. 97 (2006) 216803.
[29] L. Brey, H.A. Fertig, Phys. Rev. B 73 (2006) 235411.
[30] V. Barone, O. Hod, G.E. Scuseria, Nano Lett. 6 (2006) 2748–2754.
[31] M.Y. Han, B. Özyilmaz, Y. Zhang, P. Kim, Phys. Rev. Lett. 98 (2007) 206805.
[32] H. Sevinçli, C. Sevik, T. Çağn, G. Cuniberti, Sci. Rep. 3 (2013) 1228.
[33] J. He, T.M. Tritt, Science 357 (2017).
[34] Y. Ouyang, J. Guo, Appl. Phys. Lett. 94 (2009) 263107.
[35] H. Zheng, H.J. Liu, X.J. Tan, H.Y. Lv, L. Pan, J. Shi, x. F. Tang, Appl. Phys. Lett. 100 (2012) 093104.
[36] F. Mazzamuto, V. Hung Nguyen, Y. Apertet, C. Caër, C. Chassat, J. Saint-Martin, P. Dollfus, Phys. Rev. B 83 (2011) 235426.
[37] K.K. Saha, T. Markussen, K.S. Thygesen, B.K. Nikolić, Phys. Rev. B 84 (2011), 041412(R).
[38] H. Karamitaheri, N. Neophytou, M. Pourfath, R. Faez, H. Kosina, J. Appl. Phys. 111 (2012) 054501.
[39] Y. Yokomizo, J. Nakamura, Appl. Phys. Lett. 103 (2013) 113901.
[40] J. Cai, P. Ruffieux, R. Jaafar, M. Bieri, T. Braun, S. Blankenburg, M. Muoth, A.P. Seitsonen, M. Saleh, X. Feng, K. Mullen, R. Fasel, Nature 466 (2010) 470–473.
[41] G.Z. Magda, X. Jin, I. Hagymasi, P. Vancso, Z. Osvath, P. Nemes-Incze, C. Hwang, L.P. Biro, L. Tapaszto, Nature 514 (2014) 608–611.
[42] B. Huard, J.A. Sulpizio, N. Stander, K. Todd, B. Yang, D. Goldhaber-Gordon, Phys. Rev. Lett. 98 (2007) 236803.
[43] C.-H. Park, L. Yang, Y.-W. Son, M.L. Cohen, S.G. Louie, Nat. Phys. 4 (2008) 213–217.
[44] M. Barbier, P. Vasilopoulos, F.M. Peeters, Phys. Rev. B 81 (2010) 075438.
[45] C. Bai, X. Zhang, Phys. Rev. B 76 (2007) 075430.
[46] D. Dragoman, M. Dragoman, Appl. Phys. Lett. 91 (2007) 203116.
[47] M. Cheng, Phys. E 46 (2012) 189–192.
[48] A.F. Young, P. Kim, Nat. Phys. 5 (2009) 222–226.
[49] N. Stander, B. Huard, D. Goldhaber-Gordon, Phys. Rev. Lett. 102 (2009) 026807.
[50] P. Dollfus, V.H. Nguyen, J. Saint-Martin, J. Phys. Condens. Matter 27 (2015) 133204.
[51] A. Rahman, J.W. Guikema, N.M. Hassan, N. Markovi, Appl. Phys. Lett. 106 (2015) 013112.
[52] I.J. Vera-Marun, J.J. van den Berg, F.K. Dejene, B.J. van Wees, Nat. Commun. 7 (2016) 11525.
[53] Y.M. Zuev, W. Chang, P. Kim, Phys. Rev. Lett. 102 (2009) 096807.
[54] V.V. Cheianov, V. Fal'ko, B.L. Altshuler, Science 315 (2007) 1252–1255.
[55] P. Markos, C.M. Soukoulis, Wave Propagation: from Electrons to Photonic Crystals and Left-handed Materials, Princeton University Press, 2008.
[56] J.A. Briones-Torres, J. Madrigal-Melchor, J.C. Martínez-Orozco, I. Rodríguez-Vargas, Superlattice. Microst. 73 (2014) 98.
[57] S. Datta, Electronic Transport in Mesoscopic Systems, Cambridge University Press, 1995.
[58] H. García-Cervantes, L.M. Gaggero-Sager, O. Sotolongo-Costa, G.G. Naumis, I. Rodríguez-Vargas, AIP Adv. 6 (2016) 035309.
[59] Shakti Kumar Mishra, Amar Kumar, Chetan Prakash Kaushik, Biswaranjan Dikshit, Mater. Res. Express 5 (2018) 016301.
[60] L.-G. Wang, S.-Y. Zhu, Phys. Rev. B 81 (2010) 205444.
[61] I. Rodrguez-Vargas, J. Madrigal-Melchor, O. Oubram, J. Appl. Phys. 112 (2012) 073711.
[62] Y. Wu, V. Perebeinos, Y.-m. Lin, T. Low, F. Xia, P. Avouris, Nano Lett. 12 (2012) 1417–1423.
[63] S.J. Haigh, A. Gholinia, R. Jalil, S. Romani, L. Britnell, D.C. Elias, K.S. Novoselov, L.A. Ponomarenko, A.K. Geim, R. Gorbachev, Nat. Mater. 11 (2012) 764–767.
[64] M.C. Lemme, T.J. Echtermeyer, M. Baus, H. Kurz, IEEE Electron. Device Lett. 28 (2007) 282–284.
[65] W. Zhang, S. Brongersma, O. Richard, B. Brijs, R. Palmans, L. Froyen, K. Maex, Microelectron. Eng. 76 (2004) 146–152, Materials for Advanced Metallization 2004.
[66] B. Feng, Z. Li, X. Zhang, J. Appl. Phys. 105 (2009) 104315.
[67] S. Chen, A.L. Moore, W. Cai, J.W. Suk, J. An, C. Mishra, C. Amos, C.W. Magnuson, J. Kang, L. Shi, R.S. Ruoff, ACS Nano 5 (2011) 321–328.
[68] W. Jang, Z. Chen, W. Bao, C.N. Lau, C. Dames, Nano Lett. 10 (2010) 3909–3913.
[69] A.D. Liao, J.Z. Wu, X. Wang, K. Tahy, D. Jena, H. Dai, E. Pop, Phys. Rev. Lett. 106 (2011) 256801.
[70] B. Qiu, X. Ruan, Appl. Phys. Lett. 100 (2012) 193101.
[71] W.S. Capsinski, H.J. Maris, Physica B 219 (120) (1996) 699.
[72] T. Musho, J. Mater. Res. 30 (2015) 2628–2637.
[73] R. Venkatasubramanian, Phys. Rev. B 61 (2000) 3091–3097.
[74] M.V. Simkin, G.D. Mahan, Phys. Rev. Lett. 84 (2000) 927–930.
[75] J.-W. Jiang, J.-S. Wang, B.-S. Wang, Appl. Phys. Lett. 99 (2011) 043109.
[76] X.-K. Chen, Z.-X. Xie, W.-X. Zhou, L.-M. Tang, K.-Q. Chen, Appl. Phys. Lett. 109 (2016) 023101.
[77] S. Chen, Z. Han, M.M. Elahi, K.M.M. Habib, L. Wang, B. Wen, Y. Gao, T. Taniguchi, K. Watanabe, J. Hone, A.W. Ghosh, C.R. Dean, Science 353 (2016) 1522–1525.
[78] M.-H. Liu, C. Gorini, K. Richter, Phys. Rev. Lett. 118 (2017) 066801.
[79] V.V. Cheianov, V. Fal'ko, B.L. Altshuler, Science 315 (2007) 1252–1255.
[80] R.N. Sajjad, A.W. Ghosh, ACS Nano 7 (2013) 9808–9813.
[81] R.N. Sajjad, S. Sutar, J.U. Lee, A.W. Ghosh, Phys. Rev. B 86 (2012) 155412.
[82] S. Sutar, E.S. Comfort, J. Liu, T. Taniguchi, K. Watanabe, J.U. Lee, Nano Lett. 12 (2012) 4460–4464.